ACS APPLIED MATERIALS & INTERFACES

Research Article

www.acsami.org

TiO_2-Based Gas Sensor: A Possible Application to SO_2

Jawad Nisar,*[,†,‡] Zareh Topalian,[§] Abir De Sarkar,*[,∇,⊥] Lars Österlund,[§] and Rajeev Ahuja[†,∇]

[†]Condensed Matter Theory Group, Department of Physics and Astronomy, Uppsala University, Box 516, SE-751 20 Uppsala, Sweden

[‡]Pakistan Atomic Energy Commission (PAEC), P. O. Box. 2151, Islamabad, Pakistan

[§]Department of Engineering Sciences, The Ångström Laboratory, Uppsala University, Box 534, SE-751 21 Uppsala, Sweden

[∇]Applied Materials Physics, Department of Materials and Engineering, Royal Institute of Technology (KTH), S-100 44 Stockholm, Sweden

[⊥]Department of Physics, Central University of Rajasthan, NH-8, Bandarsindri, Rajasthan 305801, India

ABSTRACT: Fixation of SO_2 molecules on anatase TiO_2 surfaces with defects have been investigated by first-principles density functional theory (DFT) calculations and in situ Fourier transform infrared (FTIR) surface spectroscopy on porous TiO_2 films. Intrinsic oxygen-vacancy defects, which are formed on $TiO_2(001)$ and $TiO_2(101)$ surfaces by ultraviolet (UV) light irradiation and at elevated temperatures, are found to be most effective in anchoring the SO_2 gas molecules to the TiO_2 surfaces. Both $TiO_2(101)$ and $TiO_2(001)$ surfaces with oxygen vacancies are found to exhibit higher SO_2 adsorption energies in the DFT calculations. The adsorption mechanism of SO_2 is explained on the basis of electronic structure, charge transfer between the molecule and the surface, and the oxidation state of the adsorbed molecule. The theoretical findings are corroborated by FTIR experiments. Moreover, the (001) surface with oxygen vacancies is found to bind SO_2 gas molecules more strongly, as compared to the (101) surface. Higher concentration of oxygen vacancies on the TiO_2 surfaces is found to significantly increase the adsorption energy. The results shed new insight into the sensing properties of TiO_2-based gas sensors.

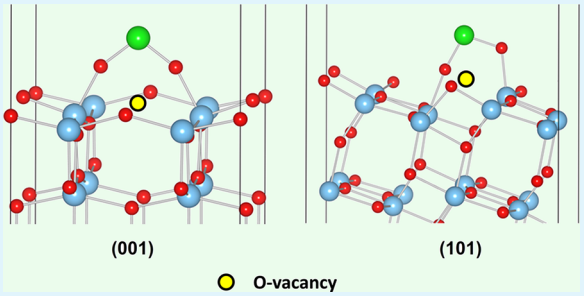

KEYWORDS: *SO_2 fixation, anatase TiO_2 surfaces, gas sensors*

1. INTRODUCTION

Titanium dioxide (TiO_2) is one of the most promising materials in a diverse array of industrial applications such as photocatalysis[1] and gas sensors.[2,3] Metal oxides, such as TiO_2, ZnO, and SnO_2,[4−8] have been widely chosen as gas-sensing materials, because of their high sensitivity, fast response, and low cost. TiO_2 exists in three different phases: rutile, anatase, and brookite. Anatase TiO_2 has hitherto drawn the most attention, especially in renewable energy and environmental applications, because of its high photocatalytic activity.[9] The anatase TiO_2 phase is also an interesting material in gas-sensing applications, because of its chemical stability. Surface defects also plays an important role in the reactivity of metal oxide surfaces[10] and detailed study of defective structures may facilitate an improvement in the overall performance of nanostructured oxides in several applications, including gas sensing.

The gas-sensing mechanism of sensors involves the adsorption of gas molecules on the metal oxide semiconductor surfaces and charge redistribution between the surfaces and the adsorbed molecules, which lead to changes in its electronic structure and conductivity. For the improvement of the performance of metal oxide gas sensors, a fundamental understanding of the interaction of molecule and surfaces is of the utmost importance. Surface defects play an important role for the adsorption of gas molecules on oxide surfaces. It is generally understood that even small concentration of defects can have substantial effects on the structural, electronic, and optical properties by inducing charge transfer between the adsorbates and the substrates. The different possible defects on oxide surfaces deserve a careful consideration for their higher utilization in controlling their surface reactivity. Charge transfer in the adsorption process underlies the gas-sensing mechanism. Oxidation or reduction of adsorbed molecules occurs because of the electronic charge transfer between the surface and the adsorbate molecule. The changes in the oxidization state of the gas molecules resulting from their adsorption on the surfaces can also be ascertained from accurate electronic structure calculations. In general, the controlled preparation of defective surfaces is very important for an atomic-level characterization of oxide surface. This is, however, experimentally very challenging. Therefore, accurate theoretical descriptions and understanding of oxide surfaces are important to enable further advancement in this field.

In this work, we have investigated the atomic and electronic structures of SO_2 adsorbed on defective $TiO_2(001)$ and $TiO_2(101)$ surfaces, using a combination of first-principles density functional theory (DFT) calculations and experimental

Received: May 22, 2013
Accepted: August 5, 2013
Published: August 5, 2013

   dx.doi.org/10.1021/am4018835 | ACS Appl. Mater. Interfaces 2013, 5, 8516−8522

methods. We have considered the most commonly occurring surface defect, namely oxygen vacancies, on both surfaces. The formation energies of defective systems are calculated at different ambient conditions (oxygen-rich and oxygen-poor). We have focused on the SO_2 gas adsorption properties on these surfaces. We have investigated the adsorption of gas molecules on TiO_2 surfaces with oxygen vacancies and found that the oxygen vacancy binds the SO_2 molecule strongly to the TiO_2 surfaces. This is verified by Fourier transform infrared (FTIR) surface spectroscopy. The calculated oxidation state of the sulfur atom is found to change upon bonding to the defective surfaces, in excellent agreement with experiments.

2. METHODOLOGY

2.1. Computational Details. The first-principles density functional theory (DFT) calculations were performed using projected augmented wave (PAW) method,[11] as implemented in the Vienna ab initio simulation package (VASP).[12] The exchange-correlation functional was treated at the level of GGA using its Perdew–Burke–Ernzerhof variant (i.e., GGA-PBE).[13] Spin-polarized DFT calculations were performed in our work. The Brillouin zone was sampled using as Monkhorst–Pack-generated set of *k*-points.[14] A *k*-points mesh with dimensions of $11 \times 11 \times 5$ and $3 \times 3 \times 1$ was determined to be dense enough to reach convergence criteria for both energy and forces. An energy cutoff of 500 eV was used for the expansion of the electronic wave function in plane wave basis. The PAW potentials with the valence states 4s and 3d for Ti, 2s and 2p for O, S have been used. In all calculations, self-consistency was achieved corresponding to a tolerance of at least 0.01 meV in the total energy. The energy of the isolated SO_2 molecule was calculated in a large cubic cell 15 Å in length. A vacuum thickness of 15 Å was used to decouple the periodic images of the slab of TiO_2 surfaces. The TiO_2 surface supercell was optimized first and later with a gas molecule adsorbed on its surface. The absorption curves is obtained from the imaginary part of the dielectric constant using Kramers–Kroning dispersion relations.[15]

2.2. Experimental Section. Nanostructured titanium dioxide films with the anatase modification were prepared by reactive DC magnetron sputtering in a deposition system based on a Balzers UTT 400 unit.[16] Two magnetron sources, arranged in an oblique angle setup, were used for sputtering Ti from 99.99% pure metallic targets. The sputter plasma was generated at a constant current of 750 mA and at a total pressure of ~40 mTorr. TiO_2 films with a thickness of ~1 μm were deposited on CaF_2 and Si(100) substrates held at room temperature. The films were characterized using a wide range of methods,[18] including X-ray photoemission spectroscopy (XPS) and grazing-incidence X-ray diffraction (GIXRD). The results from GIXRD showed that the as-deposited TiO_2 films exhibit an amorphous structure (denoted here by a-TiO_2). Subsequent annealing of the films in air at 773 K for 1 h yield highly crystalline films with distinct diffraction peaks corresponding to pure anatase structure (denoted here by c-TiO_2). No other TiO_2 phases were detected in GIXRD.

Systematic SO_2 exposures of several as-deposited and annealed films of TiO_2 were performed in a dedicated reaction cell. A gas flow of 50 ppm SO_2 in synthetic air with a total gas feed of 200 mL min^{-1} was employed. Gas exposure was made for 1 h under ultraviolet (UV) irradiation at a wavelength of 370 nm using light-emitting diode (LED) light sources with a total photon power of 1 mW cm^{-2}, and was conducted at substrate temperatures (T_s) between 293 and 673 K. Detailed information about deposition and experimental characterization of TiO_2 films and SO_2 photo-fixation can be found elsewhere.[18,28]

In situ FTIR spectroscopy was performed between 800 cm^{-1} and 4000 cm^{-1}, using a vacuum spectrometer (Bruker IFS66v/S) equipped with a liquid-nitrogen-cooled narrow-band HgCdTe detector, as previously described.[18] All FTIR measurements were carried out in transmission mode in a custom-modified reaction cell adapted for in situ reaction studies at controlled sample temperature with simultaneous FTIR spectroscopy, gas dosing, and light irradiation in a controlled atmosphere. FTIR spectra were acquired with the samples kept at T_s = 298, 373, 423, and 473 K, respectively, using a 100 mL min^{-1} gas flow of synthetic air through the reaction cell. SO_2 gas at 50 ppm was added to the gas, and the sample was irradiated with UV light, employing LED light sources of the same type as described above. Repeated IR spectra were recorded as a function of reaction time with intermittent dark and UV irradiation periods (10 min of darkness and 10 min of light). Detailed information about FTIR measurements can be found elsewhere.[18,28]

3. RESULTS AND DISCUSSION

The calculated lattice parameters—a = 3.82 Å and c = 9.66 Å—for the tetragonal structure (space group $I4_1/amd$) at the GGA-PBE level are in good agreement with experimental findings.[19] The most stable and frequently observed surfaces on anatase TiO_2 have (101) and (001) orientations[20,21] and the crystal structure of these surfaces are shown in Figure 1. The

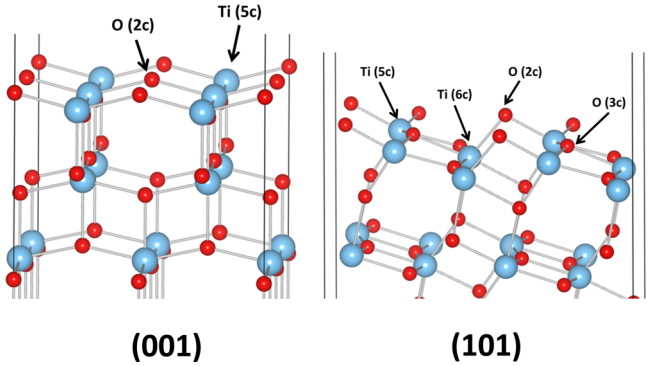

Figure 1. Optimized crystal structure of the TiO_2(001) and TiO_2(101) surfaces. Titanium and oxygen atoms are represented by blue and red spheres, respectively.

calculated surface energy of anatase TiO_2 were found to be 1.01 and 0.493 J/m^2 for the (001) and (101) surfaces, respectively. The TiO_2 (001) surface contains oxygen atoms with coordination number two (labeled O(2c) in Figure 1), while Ti has five neighboring oxygen atoms at the surface (labeled Ti(5c) in Figure 1). Similarly, in the case of TiO_2(101) surface, the atomic coordination numbers are labeled in Figure 1. The calculated band gap of anatase TiO_2 bulk, as well as the (101) and (001) surfaces, are 1.51, 1.95, and 1.35 eV, respectively, using GGA-PBE. It is well-known that the GGA-PBE functional in DFT generally underestimates the band gaps in metal oxide semiconductors.[22] GGA-PBE is however very well known for the describing the qualitative features of the electronic structure of the bulk and defective materials, and is accurate to describe relative difference.[23] It is found that the

band gap increases in the $TiO_2(101)$ surface by 29%, with respect to the bulk, while it decreases in the $TiO_2(001)$ surface by up to 10.6%, because of the quantum confinement effect. It is found that the valence band maximum (VBM) and the conduction band minimum (CBM) consist mainly of O 2p and Ti 3d states, respectively. It means that, in defect-free systems, O 2p and Ti 3d states are involved in electronic transitions across the band gap (i.e., in absorption and emission spectra).

Defects such as oxygen vacancies on metal oxide surfaces are crucially important in controlling the gas adsorption properties of anatase TiO_2. We study here the electronic and energetic properties of the anatase TiO_2 surfaces with possible neutral point defect (oxygen vacancy). O(2c) is comparatively weakly bound to the TiO_2 surfaces, because of its low coordination number. So, the energy required to remove the O(2c) atom is higher than removing the other oxygen atoms because of its higher defect formation energy. At equilibrium, the concentration of a defect in the crystal depends upon its formation energy. The defect formation energy, $\Delta E_f(D^0)$ is defined as the energy required to create an oxygen vacancy on the TiO_2 surfaces, which is calculated as follows:[8,24]

$$\Delta E_f(D^0) = E_T(D^0) - E_T(H) - \sum_\alpha n_\alpha(\mu_\alpha^{elem} + \Delta\mu_\alpha) \quad (1)$$

where $E_T(D^0)$ and $E_T(H)$ are the total energies of surfaces with and without oxygen vacancies, respectively. The term n_α is the number of the atoms of type α removed from the system to create vacancy and μ_α is the atomic potential of the corresponding atom ($\mu_\alpha = \mu_\alpha^{elem} + \Delta\mu_\alpha$). The defect formation energy depends on the chemical environmental conditions. We have investigated two extreme environments (denoted here as oxygen-rich and oxygen-poor). The chemical potentials are limited by the equilibrium condition $\Delta\mu_{Ti} + 2\Delta\mu_O = \Delta H_f(TiO_2)$, where $\Delta H_f(TiO_2)$ is the calculated formation energy of anatase TiO_2. Thus, the values for the chemical potentials can be chosen between the extreme ambient conditions such as oxygen-rich ($\Delta\mu_O = 0$) and oxygen-poor [$\Delta\mu_O = {}^1/_2\Delta H_f(TiO_2)$]. The calculated defect formation energies for these two conditions are summarized in Table 1.

Table 1. Defect Formation Energy for Anatase TiO_2 Surfaces with an Oxygen Vacancy

	Formation Energy (eV/f.u.)	
surface	oxygen-rich	oxygen-poor
$TiO_2(001)$	0.114	−0.025
$TiO_2(101)$	0.131	−0.010

It is found that the formation of oxygen vacancies on both anatase TiO_2 surfaces can be energetically favorable in the oxygen-poor condition. Under normal ambient conditions (oxygen-rich), energy is required to remove oxygen from the surface, which may be provided in the form of heat. Experimentally, it is observed that oxygen vacancies can be created on anatase TiO_2 surfaces by UV irradiation and high temperatures in an ambient environment.

The electronic structure of oxygen-deficient TiO_2 surfaces has been investigated by plotting the total and partial density of states (Figure 2). It is found that the electronic states associated with the defect appear at the bottom of conduction band (CB), and this is mainly due to Ti 3d states. It shows that oxygen vacancies in TiO_2 surfaces appear as shallow donor levels at the

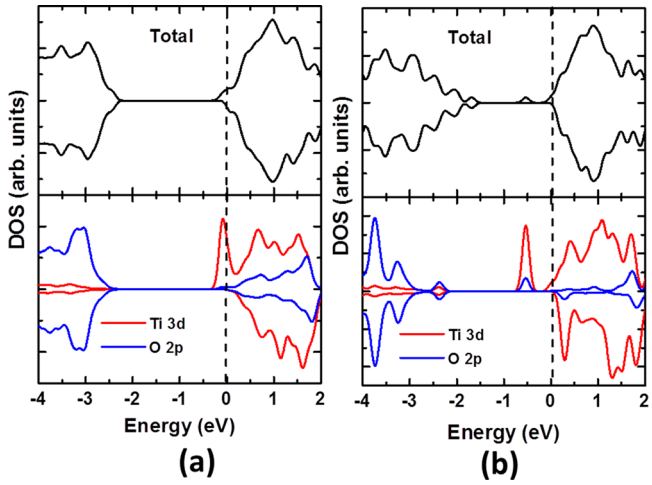

Figure 2. Total and partial density of states of anatase TiO_2 with oxygen vacancies on (a) the (101) surface and (b) the (001) surface. The vertical dashed line indicates the Fermi level.

bottom of the CB. The Fermi level is pushed toward the CB, thus resembling an *n*-type semiconductor. These electronic states may enhance the charge transfer between SO_2 molecule and the surface Ti atom. In case of the $TiO_2(001)$ surface, the energy difference between the impurity state and the CB edge is larger than that on the $TiO_2(101)$ surface. In the case of oxygen vacancies on the TiO_2 surfaces, population of the d-orbital electrons on Ti atoms adjacent to the O-vacant site increases to fulfill local charge neutrality. We found the local magnetic moment for the oxygen vacancy on the $TiO_2(001)$ and $TiO_2(101)$ surfaces to be 1.75 and 1.22 μ_B, respectively. This spin polarization occurs on the d-states of the neighboring Ti atoms, which are comparatively isotropical on the $TiO_2(001)$ surface. However, on the $TiO_2(101)$ surface, it occurs anisotropically. The Ti atoms directly affected by the creation of oxygen vacancies are polarized with a magnetic moment of 0.45 and 0.52 μ_B, while the others are polarized with a very small magnetic moment. Oxygen-deficient systems contain an excess of electrons, which form a triplet state and unpaired electrons are localized on the two Ti atoms adjacent to the oxygen-vacant site. We have compared the unpaired charge density on the $TiO_2(101)$ and $TiO_2(001)$ surfaces, which are presented in the charge distribution plots (see Figure 3). Results from a Bader analysis[25] shows that the extra charge localized on each of the two neighboring Ti(5c) atoms of oxygen-vacant site is −0.22 e on the $TiO_2(001)$ surface. In contrast, on the $TiO_2(101)$ surface the extra charge is found to be −0.25 e and −0.04 e, which is localized on the Ti(5c) and Ti(6c) atoms, respectively, adjacent to the oxygen-vacant site.

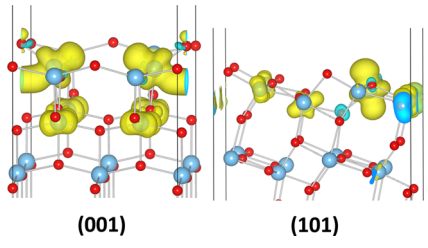

Figure 3. Partial spin charge density distribution of $TiO_2(001)$ and $TiO_2(101)$ surfaces with oxygen vacancies.

First, we have used different adsorption geometries of SO_2 molecules on pristine anatase $TiO_2(001)$ and $TiO_2((101)$ surfaces, and we have chosen the most stable configuration, based on energetic considerations. The SO_2 molecule was initialized in all possible adsorption geometries, including along the horizontal and vertical direction to the TiO_2 surfaces at different possible sites and the geometry optimization was performed for the adsorption of differently oriented SO_2 molecules at the O(2c) and Ti(5c) sites on the $TiO_2(001)$ surface and O(2c), O(3c), Ti(5c), and Ti(6c) sites on the $TiO_2(101)$ surface (shown in Figure 1). In this way, we have tried four different configurations of SO_2 molecules on different sites of the $TiO_2(001)$ surface and eight configurations on the $TiO_2(101)$ surface. We have ascertained the most stable configuration on the basis of adsorption energy (eq 2). The Ti(5c) atom is found to be the most energetically stable site for the binding of SO_2 molecule on both the $TiO_2(101)$ and $TiO_2(001)$ surfaces. Furthermore, we have calculated the adsorption energy (E_{ads}), defined as follows:[26]

$$E_{ads} = \frac{E_{slab} + nE_{SO_2} - E_{slab+SO_2}}{n} \quad (2)$$

where E_{slab}, $E_{slab+SO_2}$, and E_{SO_2} refer to the total energy of the relaxed TiO_2 surface structures, with SO_2 molecules adsorbed on the surfaces, and free SO_2 molecule in vacuum, respectively. The term n is the number of adsorbed SO_2 molecules. A positive value of E_{ads} implies that SO_2 adsorption is exothermic. The calculations show that SO_2 adsorption is exothermic on the defect-free (101) and (001) surfaces. This is confirmed by the experimentally. In FTIR experiments, only weakly bonded SO_2 molecules with a S^{4+} oxidation state are observed on anatase TiO_2 films at 298 K in air (oxygen-rich conditions).[17,27]

Defective TiO_2 surfaces can be created by heating to elevated temperatures, ion sputtering in oxygen-deficient atmospheres (typically done in vacuum preparation of TiO_2 single crystals[9]), or irradiation of UV light. The effect of UV radiation and high-temperature annealing on SO_2 adsorption has been explored experimentally by us previously.[17,27] In these studies, we have shown that SO_2 desorbs approximately above 500 K and that simultaneous O_2 exposure and UV irradiation at elevated temperature increased the SO_2 adsorption. Here, we consider oxygen-vacancy defects as a model to explain the experimental findings. While thermal creation of oxygen vacancies in TiO_2 is well-established, oxygen-vacancy formation by means of UV irradiation is less studied. When TiO_2 is irradiated with UV light, it absorbs energy and is electronically excited, with a concomitant elongation of Ti−O bonds, with respect to their ground-state values. It is highly probable that the weakest Ti−O bond on the surface is ruptured once it is stretched beyond a critical bond length. This mechanism is qualitatively corroborated by theoretical findings on excited-state properties of atomic clusters such as Si quantum dots.[28] Alternatively, UV irradiation promotes water formation on protonated TiO_2 surfaces, which is typically encountered experimentally, whereby two H−O(2c) hydroxyls condense to form water and create one oxygen vacancy. A recent electron-spin resonance study has also shown that oxygen adsorbed at oxygen-vacancy sites dissociates via sub-band-gap irradiation on reduced rutile TiO_2 nanoparticles, which was interpreted as an electron transfer mechanism from the peroxide species to a neighboring Ti^{4+} site, yielding superoxide and Ti^{3+}.[29]

Because of the symmetry of the TiO_2 surfaces, two different types of oxygen vacancies are possible on both surfaces. We have considered the oxygen vacancy, which is energetically more favorable, since the likelihood of finding such O vacancies will be correspondingly higher experimentally. The concentration of oxygen vacancies depends on the temperature of the system. When a SO_2 molecule is introduced on top of Ti cations next to the oxygen-vacancy site, it is found to cap the two Ti cations on either side of the oxygen-deficient site in a bridgelike structure, and this is shown in Figure 4. The

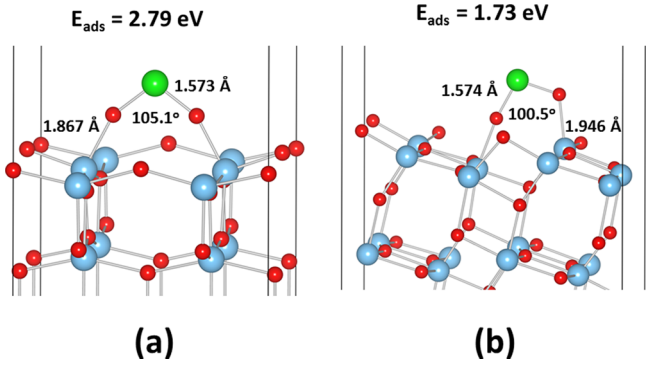

Figure 4. Single SO_2 molecule adsorbed on the defect site of anatase TiO_2: (a) (001) surface and (b) (101) surface. Ti, O, and S atoms are represented by blue, red, and green spheres, respectively.

molecular adsorption of SO_2 on both TiO_2 defective surfaces are found to be a strongly exothermic process with adsorption energies of 2.79 eV and 1.73 eV on the $TiO_2(001)$ and $TiO_2(101)$ surfaces, respectively. It implies that the adsorbed SO_2 molecule heals the Ti atoms affected by the oxygen vacancy by binding strongly to these Ti atoms (cf. Figure 3). The total magnetic moment of the $TiO_2(001)$ and $TiO_2(101)$ surfaces are restored to zero after the adsorption of the SO_2 molecules on the defective sites. The O−S−O bond angle of the SO_2 molecule is reduced to 105.1° and 100.5° after the adsorption on the (001) and (101) surfaces, respectively, which can be compared to the corresponding value for neutral gas molecule, which is 119.2°. However, the S−O bond length in SO_2 is increased to 1.57 Å, as compared to 1.45 Å in the equilibrium gas phase.

The charge-transfer mechanism between the gas molecule and the TiO_2 surfaces has been illustrated by a Bader analysis of atomic charges. The SO_2 molecule is found to bind strongly to the defect sites on the surfaces, which is indicated by the charge transferred from the Ti cations adjacent to the oxygen-deficient site to the SO_2 molecule. The charge localization on Ti induced by the oxygen vacancy is healed considerably by the SO_2 molecule. This is confirmed by a large drop in the DOS contributed by the 3d state of those Ti atoms on the defective TiO_2 surface upon SO_2 adsorption. Figure 5 shows isosurfaces of differential charge density of the SO_2 molecule adsorbed on TiO_2. The differential charge density is defined by $\Delta\rho = \rho(_{TiO_2:SO_2}) - (\rho_{TiO_2} + \rho_{SO_2})$. Here, the charge density can be either positive or negative, depending on whether an atom gains or loses charge. The charge transfer mainly involves Ti 3d, S 3p, and O 2p orbitals. The strong transfer of charge from Ti to S via O makes the Ti−O bond very stable, signifying strong bonding of SO_2 to the defect surface sites. An isosurface of differential charge density clearly shows regions of charge

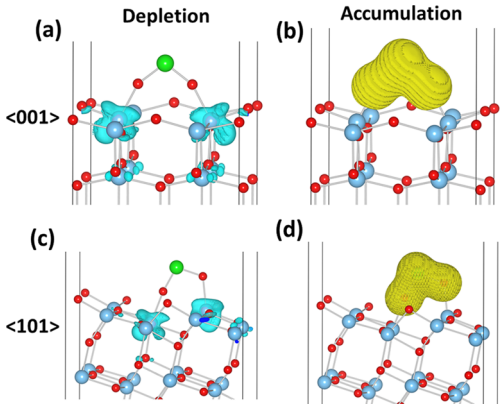

Figure 5. Isosurfaces of differential charge density, $\Delta\rho = \rho(_{TiO_2:SO_2}) - (\rho_{TiO_2} + \rho_{SO_2})$ (yellow denotes an accumulation, and cyan denotes a depletion).

depletion and accumulation. It indicates that Ti atom is no longer polarized after SO_2 adsorption.

According to the Bader analysis, the S atom gains an excess charge of 1.1 e from the neighboring Ti atoms on the (001) surface and an excess charge of 1.0 e from the neighboring Ti atoms on the (101) surface, by binding in the bridge-ike configuration to the defect sites depicted in Figure 5. The oxidation state of S is therefore reduced from +4 for the free molecule to +3 upon adsorption on the defective TiO_2 surfaces. The electronegativity of the atoms decreases in the following order: Ti > S > O. Since the O atoms in adsorbed SO_2 are already saturated with valence electrons, S draws the electronic charge from the Ti atoms via the O atoms. The gain of electronic charge can be regarded as a reduction.

A humid and oxygen-rich ambient environment is commonly encountered in experiments, which must be realistically considered in our model studies. The dissociative adsorption of H_2O and O_2 molecules on metal oxide surfaces with a high defect density is understood to occur with high likelihood, in particular at elevated temperatures and upon UV irradiation.[30,31] It is probable that atomic oxygen, originating from H_2O and/or O_2 dissociation, attaches to the reduced S atom discussed above. When one O atom binds to the adsorbed SO_2 to form a SO_3 species, the S atom is found to gain back its oxidation state (i.e., +4) at the free molecular state in the Bader analysis of atomic charges. When one additional O atom binds, it results in the formation of a SO_4 species. Upon the formation of SO_3 and SO_4, the S atom loses its electrons to the more-electronegative O atoms. In SO_4, the oxidation state of S reaches +6, as determined by the Bader charge analysis. We conclude that a mixture of SO_2, SO_3, and SO_4 species is likely to be present on the defective TiO_2 surfaces, depending on the detailed experimental conditions. Consequently, at elevated temperatures and UV irradiation, surface reactions with H_2O and O_2 are expected to promote the formation of SO_4. This explains the +6 oxidation state of sulfur found experimentally at elevated temperatures, in the presence of UV radiation.

As an experimental verification of our theoretical findings, Figure 6 shows FTIR spectra obtained after exposure to 50 ppm SO_2 in synthetic air at different T_s values with simultaneous UV irradiation. It is clear from the figure that absorption bands develop in the 1299−1372 cm^{-1} region only for $T_s \geq 373$ K, and that the main peaks consist of several overlapping bands, whose intensities gradually are redistributed

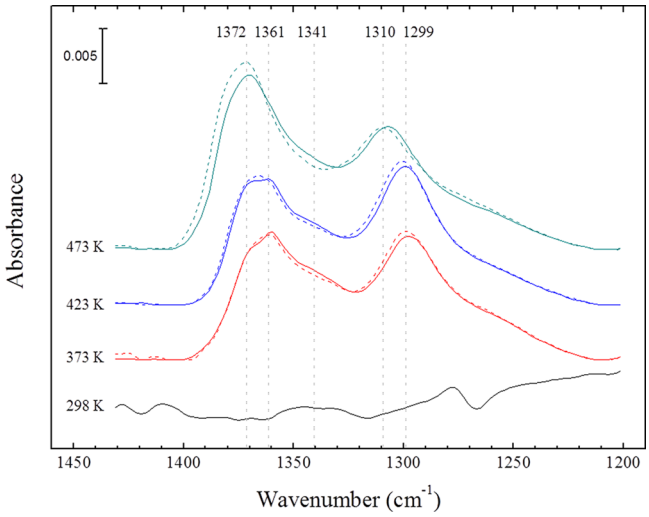

Figure 6. In situ FTIR absorbance spectra obtained in synthetic air during UV irradiation of *c*-TiO_2 films treated at different T_s values from 298 K to 473 K after 30 min (solid line) and 40 min (dashed line) of UV irradiation in 50 ppm SO_2 gas.

as a function of T_s. No SO_2-derived bands are seen at 298 K in an O-rich atmosphere in agreement with the calculations presented above. In particular, the peaks at 1299 cm^{-1} and 1361 cm^{-1} at $T_s \leq 373$ K are blue-shifted by $\Delta\bar{\nu} = 11$ cm^{-1} at $T_s = 473$ K; this is characteristic of the surface-coordinated SO_2 species.[27] These results are in good agreement with our previous results, where we have shown that UV irradiation of anatase TiO_2 films in gas containing SO_2 and O_2 at elevated temperatures results in the formation of strongly bonded SO_x species.[17,27] In these studies, it was shown that SO_2 is photo-fixated to the TiO_2 surface, and is further photo-oxidized to sulfide and sulfate surface species, where the latter are thermodynamically preferred. Results from high-resolution XPS spectra of S 2p peak binding energies show that the different possible oxidation states of sulfur on TiO_2 surfaces depend on T_s, SO_2 gas pressure, and UV irradiation.[27] Without UV irradiation, weakly bound sulfur with the S^{4+} state forms at $T_s = 298$ K on the *c*-TiO_2 films. UV irradiation at $T_s = 298$ K results in an increasing concentration of species with oxidation states S^{5+} and S^{6+}. At $T_s \geq 373$ K, films contain mainly S^{6+} species, thus proving that the photo-fixated SO_2 species are oxidized and appear as sulfate species. Together with the theoretical predictions, this strongly suggests that the FTIR spectra at $T_s \geq 373$ K in Figure 6 are due to surface-coordinated sulfate species. Furthermore, XPS measurements reveal that the sulfur concentration is 2.2 at. % for ⟨001⟩-oriented films and 1.98 at. % for ⟨101⟩-oriented films. Even if this difference is small (11%), the porosity of the ⟨101⟩ films is higher and strongly suggests that the SO_2 adsorption energy is higher on the defect (001) surface, as compared to the corresponding (101) surface, in good agreement with the DFT results.

In order to further investigate the chemisorption of SO_2 molecule on the (001) and (101) surfaces and elaborate on the adsorption phenomena, the electronic structure of the surface with an adsorbed SO_2 molecule is investigated by plotting the partial density of states (Figure 7). Figure 7 clearly shows that charge is transferred from the Ti 3d states to the SO_2 molecule. In case of the (001) surface, the occupied states appear 0.4 eV below the conduction band (CB), which is due to the S 3p and

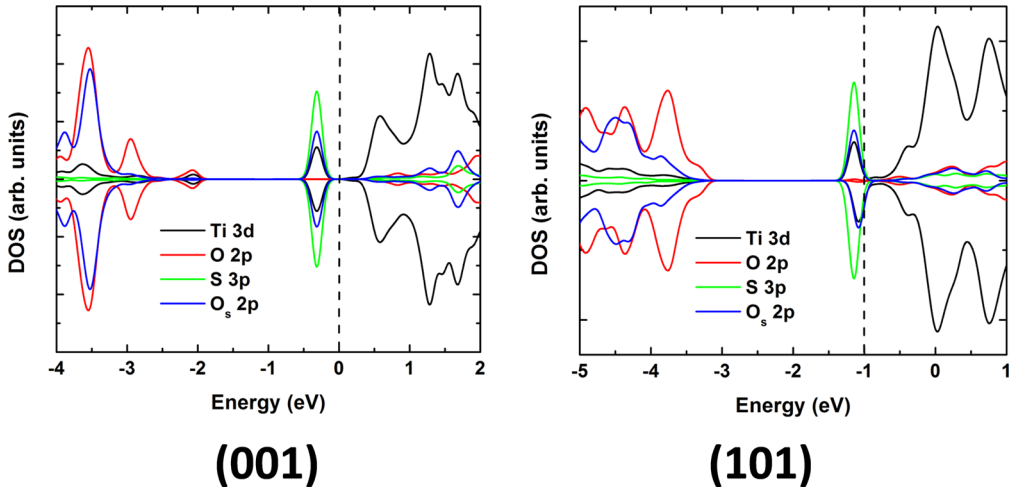

Figure 7. Partial density of states of SO_2 adsorbed on anatase $TiO_2(001)$ and $TiO_2(101)$ surfaces with oxygen vacancies.

O_s 2p states, and the valence band (VB) is slightly shifted upward by 0.11 eV, with respect to the clean surface. In this way, the band gap is drastically reduced due to appearance of occupied states below the Fermi level. It indicates that conductivity is increased upon SO_2 chemisorption on defective (001) surfaces. In the case of the (101) surface, the occupied states which appear close to the edge of the CBM and found to have merged with the conduction band. These states are composed of the 3p states of sulfur and surface oxygen O_s 2p, respectively). Partially filled states appear at the Fermi level, which shows metallic behavior. Thus, it is observed that the electronic property of the surface has changed from semiconducting to metallic, because of the adsorption of SO_2 molecule on the defective $TiO_2(101)$ surface. TiO_2 surfaces are highly sensitive and, therefore, useful for SO_2 gas sensing, because of high adsorption energy and drastic change in the electronic structure. This is confirmed by the calculated absorption spectra. It is observed that the edge of the absorption spectra shifts to lower energies (Figure 8), which enhances the conductivity.

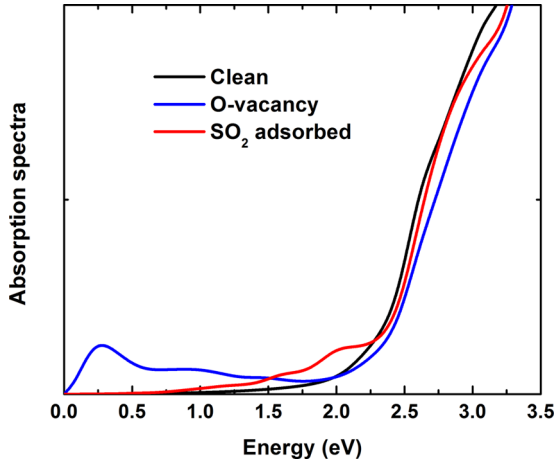

Figure 8. Absorption spectra of defect-free $TiO_2(001)$ surface, $TiO_2(001)$ surface with oxygen vacancies, and SO_2 gas molecule adsorbed on the defect $TiO_2(001)$ surface.

4. CONCLUSIONS

In this work, we have focused on the adsorption of SO_2 gas molecule on defect anatase TiO_2 surfaces for the purpose of exploring the SO_2 gas sensory functionality of the latter. Ultraviolet (UV) radiation and elevated temperatures induce the formation of defects (i.e., oxygen vacancies) on the TiO_2 surfaces. The electronic structure of both the defective TiO_2 surfaces and the SO_2 molecules adsorbed on it has been investigated by first-principles density functional theory (DFT) calculations. In our combined experimental and theoretical studies, the surface defects are found to be important and necessary to adsorb and sense the SO_2 gas molecules. Oxidation state of sulfur changes from +4 on the free molecule to +3 upon its adsorption on $TiO_2(001)$ and $TiO_2(101)$ surfaces at the defective sites. However, the consideration of humid and oxygen-rich environments, commonly occurring in experiments opens the possibility for atomic O to bind to the adsorbed SO_2 to form SO_3 and SO_4. This atomic O arises due to the facile dissociation of ambient H_2O and O_2 molecules on defective TiO_2 surfaces. In the formation of SO_3 and SO_4 S atom loses its electrons to the more-electronegative O atoms. Consequently, in SO_3 and SO_4, the oxidation state of S reaches +5 and +6, respectively, as determined by the Bader analysis of atomic charges in our DFT calculations, which is confirmed by XPS.

AUTHOR INFORMATION

Corresponding Author

*E-mail addresses: jawad.nisar124@gmail.com (J.N.), abirdesarkar@gmail.com (A.D.S.).

Notes

The authors declare no competing financial interest.

ACKNOWLEDGMENTS

We would like to acknowledge the Swedish Research Council (VR and FORMAS), Stiffelsen J. Gust Richerts Minne (SWECO), and Swedish Energy Agency (Energimydigheten) for financial support. J.N. is thankful to the Higher Education Commission (HEC) of Pakistan for financial support. The Postdoctoral Fellowship support from the Wenner-Gren Stiftelserna/Foundation and the EU Grinddoor project is gratefully acknowledged by A. De Sarkar and Z. Topalian, respectively. SNIC and UPPMAX are acknowledged for providing computing time.

REFERENCES

(1) Fujishima, A.; Zhang, X. T.; Tryk, D. A. *Surf. Sci. Rep.* **2008**, *63*, 515−582.
(2) Varghese, O. K.; Grimes, C. A. *J. Nanosci. Nanotechnol.* **2003**, *3*, 277−293.
(3) Sorescu, D. C.; Al-Saidi, W. A.; Jordan, K. D. *J. Chem. Phys* **2011**, 135.
(4) Yuan, Q.; Zhao, Y.-P.; Li, L.; Wang, T. *J. Phys. Chem. C* **2009**, *113*, 6107.
(5) Chen, Y. J.; Xue, X. Y.; Wang, Y. G.; Wang, T. H. *Appl. Phys. Lett.* **2005**, 87.
(6) Batzill, M.; Diebold, U. *Phys. Chem. Chem. Phys.* **2007**, *9*, 2307−2318.
(7) Wanbayor, R.; Ruangpornvisuti, V. *Mater. Chem. Phys.* **2010**, *124*, 720−725.
(8) Nisar, J.; Araujo, C. M.; Ahuja, R. *Appl. Phys. Lett.* **2011**, *98*.
(9) Diebold, U. *Surf. Sci. Rep.* **2003**, *48*, 53−229.
(10) Gong, X. Q.; Selloni, A.; Batzill, M.; Diebold, U. *Nat. Mater.* **2006**, *5*, 665−670.
(11) Blochl, P. E. *Phys. Rev. B* **1994**, *50*, 17953−17979.
(12) Kresse, G.; Joubert, D. *Phys. Rev. B* **1999**, *59*, 1758−1775.
(13) Perdew, J. P.; Chevary, J. A.; Vosko, S. H.; Jackson, K. A.; Pederson, M. R.; Singh, D. J.; Fiolhais, C. *Phys. Rev. B* **1992**, *46*, 6671−6687.
(14) Monkhorst, H. J.; Pack, J. D. *Phys. Rev. B* **1976**, *13*, 5188−5192.
(15) Gajdos, M.; Hummer, K.; Kresse, G.; Furthmuller, J.; Bechstedt, F. *Phys. Rev. B* **2006**, 73.
(16) Lebellac, D.; Niklasson, G. A.; Granqvist, C. G. *J. Appl. Phys.* **1995**, *77*, 6145−6151.
(17) Topalian, Z.; Niklasson, G. A.; Granqvist, C. G.; Osterlund, L. *Thin Solid Films* **2009**, *518*, 1341−1344.
(18) Mattsson, A.; Leideborg, M.; Larsson, K.; Westin, G.; Osterlund, L. *J. Phys. Chem. B* **2006**, *110*, 1210−1220.
(19) Cromer, D. T.; Herrington, K. *J. Am. Chem. Soc.* **1955**, *77*, 4708−4709.
(20) Yang, H. G.; Sun, C. H.; Qiao, S. Z.; Zou, J.; Liu, G.; Smith, S. C.; Cheng, H. M.; Lu, G. Q. *Nature* **2008**, *453*, 638−U4.
(21) Zhang, J. L.; Zhang, M.; Han, Y.; Li, W.; Meng, X. K.; Zong, B. N. *J. Phys. Chem. C* **2008**, *112*, 19506−19515.
(22) Godby, R. W.; Schluter, M.; Sham, L. J. *Phys. Rev. Lett.* **1986**, *56*, 2415−2418.
(23) Gai, Y.; Li, J.; Li, S. S.; Xia, J. B.; Wei, S. H. *Phys. Rev. Lett.* **2009**, *102*, 036402.
(24) Nisar, J.; Arhammar, C.; Jamstorp, E.; Ahuja, R. *Phys. Rev. B* **2011**, 84.
(25) Bader, R. *Atoms in Molecules: A Quantum Theory*; Oxford University Press: New York, 1990.
(26) Nisar, J.; Araujo, C. M.; Ahuja, R. *Surf. Sci.* **2010**, *604*, 617−622.
(27) Topalian, Z.; Niklasson, G. A.; Granqvist, C. G.; Osterlund, L. *ACS Appl. Mater. Interfaces* **2012**, *4*, 672−679.
(28) Zhang, R. Q.; De Sarkar, A.; Niehaus, T. A.; Frauenheim, T. *Phys. Status Solidi B* **2012**, *249*, 401−412.
(29) Komaguchi, K.; Maruoka, T.; Nakano, H.; Imae, I.; Ooyama, Y.; Harima, Y. *J. Phys. Chem. C* **2010**, *104*, 1240.
(30) Henrich, V. E. *Rep. Prog. Phys.* **1985**, *48*, 1481−1541.
(31) Smith, K. E.; Mackay, J. L.; Henrich, V. E. *Phys. Rev. B* **1987**, *35*, 5822−5829.